Bioelectrochemistry 145 (2022) 108057

Contents lists available at ScienceDirect

Bioelectrochemistry

journal homepage: www.elsevier.com/locate/bioelechem

Development of a biosensor for phosphorylated Tau 181 protein detection in Early-Stage Alzheimer's disease

Maria Eduarda Schneider [a,b], Lucía Guillade [d], Miguel A. Correa-Duarte [c,d], Felismina T.C. Moreira [a,b,*]

[a] BioMark/ISEP, School of Engineering, Polytechnic Institute of Porto, Portugal
[b] CEB, Centre of Biological Engineering, Minho University, Braga, Portugal
[c] Department of Physical Chemistry, Center for Biomedical Research (CINBIO), Southern Galicia Institute of Health Research (IISGS), Spain
[d] Biomedical Research Networking Center for Mental Health (CIBERSAM), Universidade de Vigo, Vigo 36310, Spain

ARTICLE INFO

Article history:
Received 2 December 2021
Received in revised form 10 January 2022
Accepted 11 January 2022
Available online 14 January 2022

Keywords:
Alzheimer
Biomarker
Electrochemical
Immunosensor

ABSTRACT

Alzheimer's disease (AD) is the most common form of dementia in the elderly, and there are still no reliable methods for its early detection. Recently, the phosphorylated protein Tau181 (p-Tau181) was identified as a highly specific biomarker for AD. Therefore, in this work, a new strategy for the development of an electrochemical-based immunosensor for the detection of p-Tau181 is described. For this purpose, a carbon screen-printed electrode (C-SPE) was modified with platinum nanoparticles decorated with multi-walled carbon nanotubes (MWCNTs- PAH /Pt) to enable antibody binding. Scanning electron microscopy, transmission electron microscopy, Raman and X-ray photoelectron spectroscopy were used to study the morphology and crystallinity of the nanomaterials. Cyclic voltammetry and square-wave voltammetry were performed to compare the electrochemical properties of these electrodes. Under optimal conditions, the developed immunosensor exhibited a linear range from 8.6 to 1100 pg/mL, and the detection limit was estimated to be 0.24 pg/mL. This device showed excellent reproducibility and stability with remarkable selectivity for p-Tau181 in serum samples. Overall, this device enables minimally invasive clinical evaluation of p-Tau181 level with high sensitivity through simple operation, which makes this device a promising tool for future point-of-care purposes that will contribute to the technological development of clinical diagnostics.

1. Introduction

Alzheimer's disease (AD) is one of the most common forms of dementia, attacking the brain and affecting memory, behaviour and emotions. There are currently more than 50 million cases of dementia, and this number is expected to double every 20 years [1–3]. This increase is due to the ageing of the world's population and is an imminent public health problem. Diagnosis of AD is currently costly and invasive, with accurate diagnosis only possible by autopsy [4–6]. Pathologically, AD is defined by the accumulation of amyloid plaques and intracellular neurofibrillary tangles, which are the result of microtubule non-stabilisation due to abnormal accumulation of hyperphosphorylated Tau protein [7–9], leading to aggregation and consequent neuronal dysfunction [10]. There is evidence that this accumulation begins years before the clinical symptoms of AD appear, allowing for early diagnosis.

The identification of biomarkers for AD has been subject of studies for many years, mostly based on the analysis of cerebrospinal fluid or positron emission tomography images (PET) [11,12]. Recent studies show that Tau protein is an important biomarker for early diagnosis of AD via blood, and confirmed that Tau phosphorylated at threonine 181 (p-Tau181) is very specific for AD [13]. Mass spectrometry [14], western blot [15], PET images [16], immunomagnetic reduction [17], and immunoassays [18–20] are the existing gold standard methods that can accurately detect and quantify p-Tau181. In the specific case of blood immunoassays targeting Tau species, particularly Tau fragments phosphorylated at threonine 181, these assays have shown promising results, demonstrating that they are a reliable tool for AD diagnostic. However, the described methods have some limitations, such as false positive and negative results, interpretation problems, complexity, time consumption and expensive equipment. Therefore, there is a need to develop a new diagnostic method that allows accurate,

* Corresponding author at: BioMark Sensor Research/ISEP, School of Engineering of the Polytechnic School of Porto, R. Dr. António Bernardino de Almeida, 431, Porto 4249-015, Portugal.
E-mail address: ftm@isep.ipp.pt (F.T.C. Moreira).

https://doi.org/10.1016/j.bioelechem.2022.108057
1567-5394/

rapid, and cost-effective early detection of AD with minimally invasive procedures.

One promising technology is based on electrochemical immunosensors, which combines the accuracy of electrochemical assays with the selectivity of an antibody as a biorecognition element [21–23].Various molecules such as antibodies[24–26], aptamers[27], or plastic antibodies [28] with promising operational properties have been used to detect the Tau protein. Nevertheless, biosensors still need to be improved in terms of sensitivity and selectivity. This could be attained through the use of nanomaterials, which are also being integrated into biosensor analytical instrumentation to create more sensitive and highly accurate biosensing platforms. Various types of nanomaterials such as gold nanoparticle [25,26], magnetic nanoparticles [25], quantum dots [29], and carbon nanotubes [30] have been integrated into biosensor platforms for Tau protein detection due to their unique chemical and physical properties.

Almost all electrochemical biosensors for the detection of Tau protein described in the literature are based on an antibody as a biorecognition element. Tau-441 was detected in the work of Carlin and Martic-Milne [31]. The authors developed a very easy to fabricate gold electrode coated with anti-Tau antibody. Later, Wang and co-authors fabricated a four-electrode system of gold microband electrodes coated with a self-assembling monolayer and protein G. Protein G is used to interact with the immobilized antibodies and ensure their optimal alignment [19]. This work showed a good detection limit of 0.03 fM but uses an additional protein (protein G) to develop the sensing layer, implying a more expensive and complex assay. Another assay was later developed by Karaboga and Sezginturk (2020), who presented a more complicated design of indium tin oxide electrodes coated with polyethylene terephthalate and using a nanocomposite of reduced graphene oxide and gold nanoparticles for antibody binding. [32] Another interesting paper was published by Razzino and co-authors who described in 2020. They reported a C-SPE modified with a nanocomposite of gold nanoparticles and poly(amidoamine) dendrimers, and the attachment of an anti-Tau antibody to detect Tau protein. The biosensor showed good analytical performance in terms of detection limit (1.7 pg/mL), but this method is complex because a second labelled antibody is required[26]. In general, the use of nanocomposite structures in the design of biosensors significantly increases the sensitivity of the sensor and decrease the detection limit. Carbon nanotubes (CNTs) are widely used for biosensing because they have a large surface area and good electrocatalytic properties [33]. To increase the performance of the device, the multi-walled carbon nanotubes (MWCNTs) can be combined with other materials, making the nanocomposite more efficient than using individual components. Nanoparticles with a stable physicochemical structure, such as gold and platinum, are often used to modify the electrode or antibody surface to enhance the signal.

Therefore, in this study, a simple and novel electrochemical immunosensor was developed for the determination of p-Tau181 protein in serum. In this approach, a C-SPE modified with a layer of aminated carbon nanotubes coated with platinum nanoparticles (MWCNTs- PAH /Pt) was used, which serve as a binding layer for the antibodies because they have affinity and enhance electron transfer. The detection of this immunosensor occurs after the binding of p-Tau181, which changes the electrochemical signals that are analyzed by square wave voltammetry (SWV). The analytical performance of the immunosensor was tested with spiked serum. Overall, this methodology contributes to an accurate, cost-effective and simple method for the diagnosis of AD.

2. Materials and methods

2.1. Reagents

All solutions were prepared in ultrapure water Milli-Q. Sodium chloride (NaCl) poly(allylamine hydrochloride) (PAH), sodium borohydride ($NaBH_4$), sodium citrate tribasic dihydrate, 98% and chloroplatinic acid hydrate (H_2PtCl_6-xH_2O, 99.9%), potassium ferricyanide III ($[K_3[Fe(CN)_6]$), potassium ferricyanide II ($[K_4[Fe(CN)_6]$) trihydrate, hemoglobin, potassium chloride (KCl), phosphate buffered saline (PBS, 0.01 M, pH 7.4), bovine serum albumin (BSA) and fetal bovine serum (FBS) were purchased from Sigma Aldrich. Glycerol and DL-dithiothreitol were used for the p-Tau181 buffer preparation. Tau [p-Tau181] and polyclonal antibody (Thr181) were purchased from Invitrogen. Interfering solutions to selectivity tests were prepared in PBS under physiological conditions, in this case Igg, hemoglobin, uric acid and BSA.

2.2. Equipment and materials

Screen-printed electrodes (SPE) (Dropsens DRP-C110) with a 4 mm diameter carbon working electrode, a carbon counter electrode, and an Ag pseudoreference electrode in a ceramic strip (dimensions 3.4 x1.0 x 0.05 cm) were used for all experiments. Electrochemical measurements were performed in a Metrohm Autolab potentiostat/galvanostat controlled by NOVA 1.11 software.

Raman spectra were recorded for the chemical analysis of the sensor in a Thermo Scientific DXR Raman using a confocal microscope and a 532 nm excitation laser.

The surface morphology of the different samples was determined using a field emission scanning electron microscope (FESEM, JEOL-JSM −6700F) equipped with a retractable backscatter electron detector and a detector from the Oxford Inca EDX system for compositional analysis. Another technique for the morphology analysis was transmission electron microscope (TEM, JEOL-JEM 1010) with an accelerating voltage of 100 kV. High-resolution transmission electron microscopy (HRTEM) was performed with a microscope (JEOL-JEM 2010F) at 200 kV (accelerating voltage).

XPS measurements were performed with monochromatic Al-Ka radiation (hn = 1486.6 eV). Photoelectrons were collected at a collection angle of 90° relative to the sample surface. The measurement was performed in constant analyzer energy mode with a pass energy of 100 eV for overview spectra and 20 eV for high-resolution spectra. Charge referencing was performed by setting the C1s photopeak with lower binding energy to 284.8.0 eV C1s hydrocarbon peak. The elemental composition of the surface was determined using standard Scofield photoemission cross sections. Samples were analyzed using a Thermo Scientific K-Alpha ESCA instrument equipped with monochromatic aluminum Kα radiation at an X-ray source of 1486.6 eV.

2.3. Synthesis of MWCNTs-PAH/Pt

For functionalization of CNTs with (poly)electrolytes, multi-walled carbon nanotubes (MWCNTs, Nanolab, 5–20 μm in length and 10–15 nm in diameter) were sonicated in a mixture of acetone/EtOH (1:1, 20 mL) for 10 min and centrifuged three times (9000 rpm, 20 min) before (re)dispersion in ultrapure water (18 $M\Omega\ cm^{-1}$). The sample was then freeze-dried for 48 h and used without further treatment (13). CNTs (7.5 mg) were dispersed in an aqueous 0.5 M NaCl solution (50 mL) containing 1 wt% polyallylamine hydrochloride (PAH) to a final concentration of 150 mg/L.

The pH of the solution was adjusted to 9.5 to promote coating of the MWCNTs by PAH. The resulting mixture was magnetically stirred (1 h) and then sonicated with an ultrasonic probe (3 h) to ensure dispersion. The excess of PAH was removed by 3 centrifugation cycles (12000 rpm, 24 h) and redispersed by sonication in water. The CNT concentration was determined to be 0.6 mg/mL after absorbance measurement and substitution by a calibration curve. Spherical platinum nanoparticles were synthesized using $NaBH_4$ (2.45 mL, 0.015 M) rapidly injected into a solution of sodium citrate tribasic dihydrate (2.5 mL, 0.1 M) and chloroplatinic acid hydrate (2.5 mL, 0.05 M) in H_2O (43 mL) at room temperature (molar ratio $Na_3C_6H_5O_7/H_2PtCl_6/NaBH_4$ 2:1:0.3). The resulting solution was stirred for 15 min and yielded 2–5 nm Pt-NPs (brown color). The final step was to deposit the NPs on MWCNTs by adding MWCNTs PAH (0.25 mL, 0.6 mg/mL) to 25 mL of Pt-NPs solution (0.5 mM). After stirring for 30 minutes, the dispersion was centrifuged several times (9000 rpm, 1 h) and redispersed in 5 mL H_2O containing 0.03 mg/mL MWCNTs.

2.4. Immunosensor assembly

The immunosensor was assembled on the C-SPE in several steps, as shown in Fig. 1. First, the C-SPE was pre-treated by chronoamperometry at + 1.7 V for 200 seconds in KCl (0.1 M). Then the electrode was washed with ultrapure water, and the nanoparticles (MWCNTs-PAH/Pt) were dropped onto the working electrode. This incubation was performed three times during 30 minutes at 60 °C. Then, the antibody was dropped on the electrode surface at an optimized concentration (1 mg/mL) for 2 hours. To block nonspecific binding sites on the electrode surface, the device was incubated with BSA (0.01%) for 30 min. The final step consisted of a 30minutes incubation with p-Tau181 at various concentrations. As a control, C-SPEs were fabricated without PtNP and with dendritic PtNP, following the same steps as previously described but without MWCNTs-PAH /Pt and with carbon nanotubes only. All steps of the electrode assembly were monitored by SWV and cyclic voltammetry (CV).

2.5. Electrochemical measurements

All electrochemical tests were monitored using the response of the redox probe 5 mM $[Fe(CN)_6]^{3-/4-}$ prepared in 0.1 M KCl, which triggers an electron transfer process at the C-SPE surface and allows surface characterization by techniques such as CV and SWV. In these experiments, potentials from −0.4 to + 0.6 V were scanned at 0.050 V/s. These analyzes can be used to verify how the modification of the electrode surface affects the redox processes of the probe.

Calibration curves were constructed to test the binding of p-Tau181 after 30 min incubation with concentrations ranging from 8.6 to 1100 pg/mL in DTT-glycerol and FBS diluted 1:100 and 1:10 in DTT-glycerol. The spiked serum samples were diluted 10- fold before spiking p-Tau181 protein at a concentration of 7.8 pg/mL, 17.6, 7.8 pg/mL and 1.0 ng/mL, respectively.

3. Results and discussions

3.1. Immunosensor assembly

The immunosensor was constructed according to the steps described in Fig. 1, which include (A) pre-treatment, (B) immobilization of the MWCNTs PAH /Pt, (C) antibody binding, and (D) incubation with BSA to block nonspecific interactions. All these steps were analyzed using CV **(**Fig. 2**A)** and SWV **(**Fig. 2**B)** to track the progress in each immobilization stage. The addition of MWCNTs-PAH/Pt, served to prepare the electrode for the immobilization of the antibody, since the nanocomposite contains amine groups.

The CV spectra of MWCNTs-PAH /Pt shows a significant increase in current compared to bare C-SPE, indicating that the nanocomposite facilitates the redox process of the iron probe on the C-SPE surface, an expected behavior since platinum is considered an excellent electrical conductor. After immobilization of the anti-p-Tau181 antibody, the current value decreased significantly, indicating that the binding of the antibody was successful. This decrease in current and increase in peak-to-peak separation are related to the formation of a barrier to the electrons transfer at the interface between the redox probe and the electrode surface. In this case, the antibody, which is a larger molecule, contributes to the decrease in electron transfer across the electrode surface.

The immobilization of the antibody on the surface of the immunosensor is considered key for a good development of the device and can be done in a specific or random way. Different types of immobilization can be found in the literature, in this case, random adsorption on the surface was chosen, a direct approach known as *flat-on* [34]. Adsorption of biomolecules on water-insoluble surface-active supports is probably the most economically attractive method of immobilization because it is simple

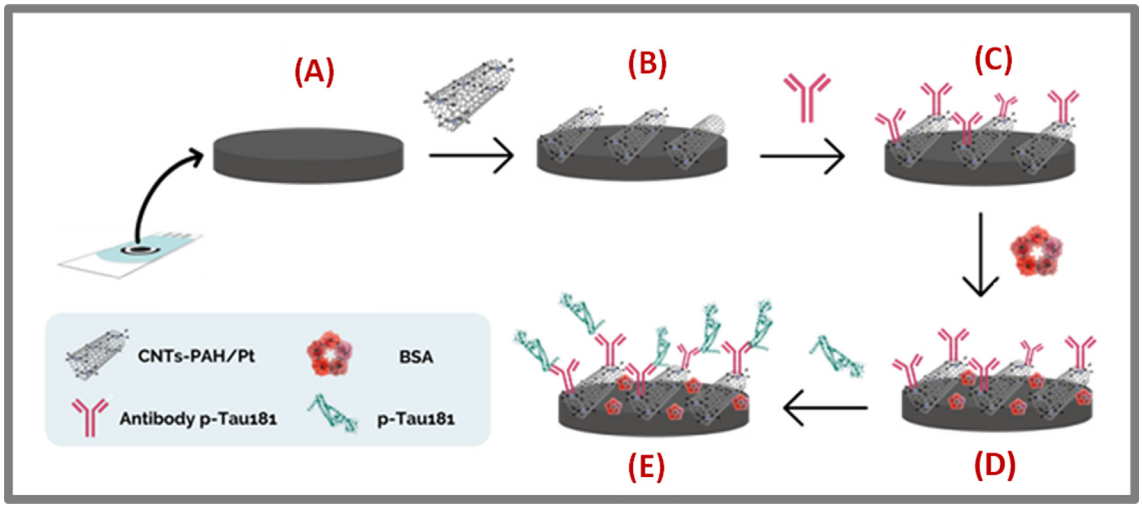

Fig. 1. Different steps for fabrication of p-Tau181 immunosensor.

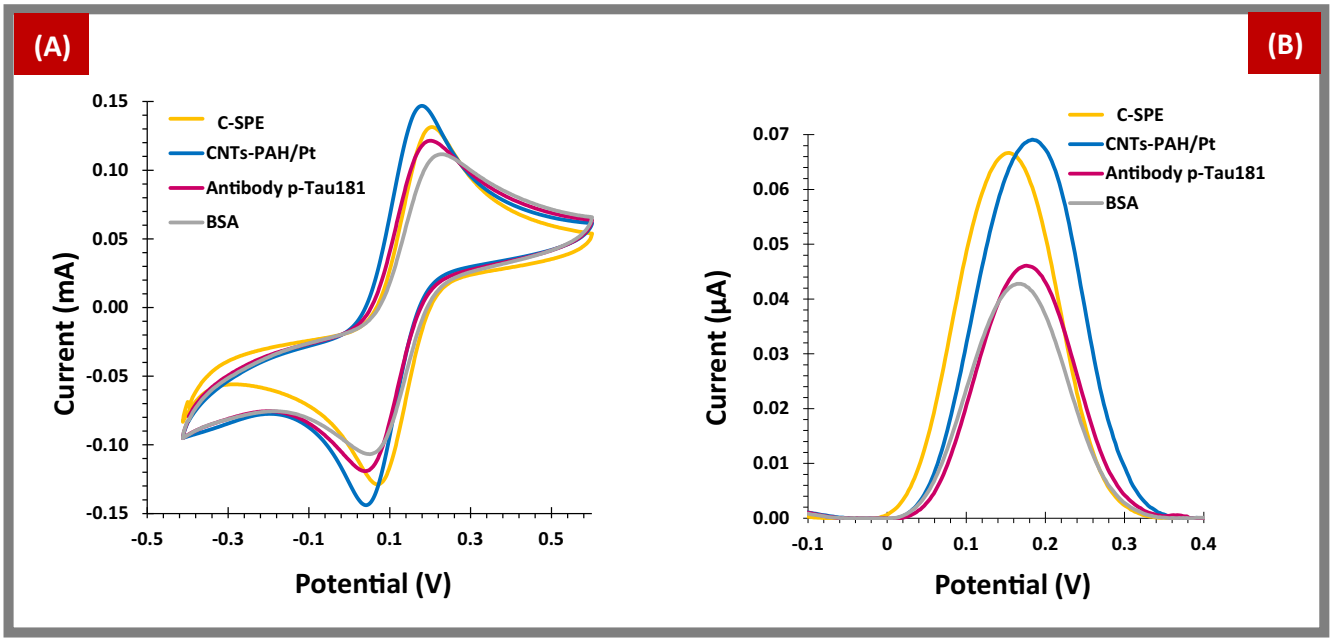

Fig. 2. (A) CV of (yellow) bare C-SPE, (blue) C-SPE / MWCNTs-PAH/Pt, (red) C-SPE / MWCNTs-PAH/Pt/ antibody, (grey) C-SPE / MWCNTs-PAH/Pt/antibody/BSA in PBS 0.1 M (pH 7.5) containing 5 mM $[Fe(CN)_6]^{3-/4-}$ prepared in KCl 0.1 M at scan rate 50 mVs^{-1} . (B) SWV (yellow) bare C-SPE, (blue) C-SPE / MWCNTs-PAH/Pt, (red) C-SPE / MWCNTs-PAH/Pt / antibody, (grey) -SPE / MWCNTs-PAH/Pt / antibody/BSA in PBS 0.1 M (pH 7.5) containing 5 mM $[Fe(CN)_6]^{3-/4-}$ prepared in KCl 0.1 M at scan rate 50 mVs^{-1}. (For interpretation of the references to color in this figure legend, the reader is referred to the web version of this article.)

and inexpensive. This method is interesting when the proteins are not stable as in covalent or (bio)affinity binding. In this approach, antibody immobilization is based on intermolecular forces such as electrostatic, hydrophobic, van der Waals, and hydrogen bonding interactions or a combination of them [35]. Hydrogen bonding and electrostatic interactions are expected to predominate once the composite is composed of aminated MWCNTs modified with Pt, and consequently the amines should interact with the $–COO^-$ group of the antibody. The last step was to block all non-specific binding to avoid positive bias, and a BSA solution was used for this purpose, resulting in a current decrease.

The SWV measurements **(**Fig. 2**B)** agree with the data from CV. After applying the nanomaterial to the C-SPE surface, an increase in peak current was observed due to the conductive properties of the nanomaterial. A decrease in peak current was then observed after the attachment of antibodies and the blocking step, which is expected once the biomolecules form a barrier to electron transfer.

3.2. Physicochemical characterization of nanostructures

3.2.1. Transmission electron microscope

The morphology of the nanocomposite was characterized by HRTEM as shown in Fig. 3**.** The size, shape, distribution and aggregation of the nanoparticles on the MWCNT network were also studied HRTEM. These images show the structure of the carbon nanotubes **(**Fig. 3**A),** which form a kind of network in which the aminated platinum particles are uniformly distributed between the MWCNT **(**Fig. 3**B).** These particles are 2–5 nm in diameter and provide a large surface area for the immobilization of biomolecules. Fig. 3 shows that the nanoparticles have good dispersibility, have a homogeneous surface area and exhibit a uniform spherical morphology. The controlled size of the nanoparticles plays an important role as it can significantly improve the electrochemical conductivity of the nanocomposite compared to non-dispersed or inhomogeneous nanoparticles. The platinum particles are aminated with weak cationic polyelectrolytes with many amino groups, this combination favors the assembly of the immunosensor.

3.2.2. Scanning electron microscope

The surface morphology of the MWCNTs-PAH /Pt composite and the MWCNTs-PAH /Pt modified with anti-Tau181 antibody was investigated using SEM. The electrode surface was mostly covered with homogeneous MWCNTs in the form of small tubular bundles **(**Fig. 4**).** The presence of the nanoparticles was clearly visible on the surface of the composite-modified C-SPE, indicating that they were bound to the MWCNTs. As shown in Fig. 4**B**, the morphology of the surface changed significantly after immobilization of the antibody on the MWCNTs PAH /Pt composite due to the interaction between the nanocomposite and the antibody molecules. In addition, the distribution of the antibody throughout the structure of the MWCNTs-PAH /Pt composite may have led to the formation of electrostatic interactions between the antibody and the Pt nanoparticles.

3.2.3. X-ray photoelectron spectroscopy

The chemical states of the MWCNTs-PAH/Pt, MWCNTs-PAH/Pt modified with the antibody, and after binding the p-Tau181 protein were detected by XPS. The chemical composition and chemical environment of the sample were examined ex situ by XPS surface. C1s, O1s, and survey spectra were recorded during the measurements. The experimental XPS data used to prepare the analytical summary are shown in Fig. 5. A broad analytical spectrum is used to identify and quantify all elements on the surface of the sample. Overall, this chemical analysis is used to verify the chemical changes on the surface caused by the deposition of different layers of materials on the C-SPE surface (Fig. 5).

Fig. 5 shows that when the MWCNTs-PAH/Pt were dropped onto the electrode surface, platinum and CNTs were detected, which was expected since these elements are present in the nanocomposite material. When the antibody is attached, the oxygen content increases due to the oxygen and nitrogen in the high molecular weight protein, and sodium is also detected, which is

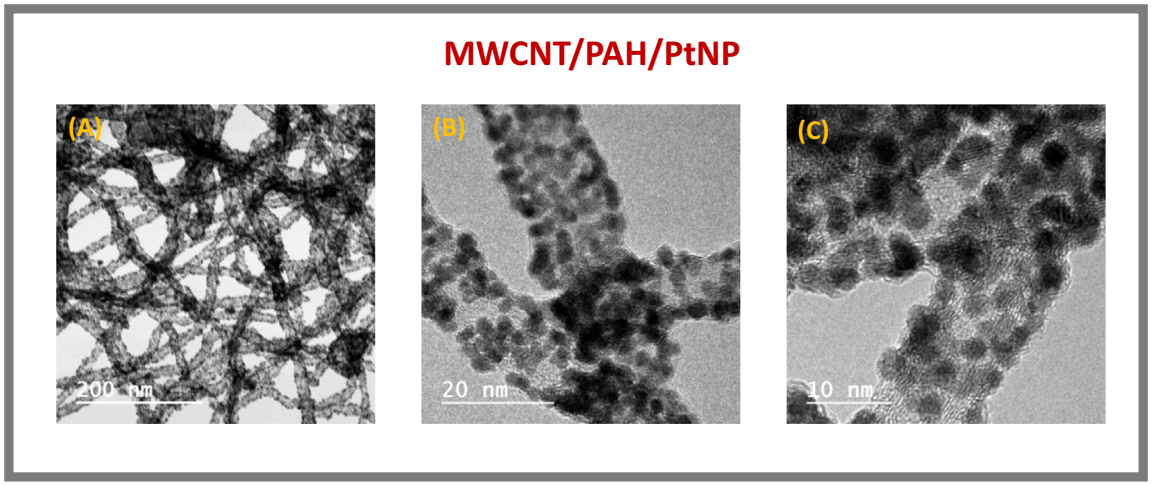

Fig. 3. High resolution transmission electron microscopy analysis of the composite material, MWCNTs-PAH/Pt.

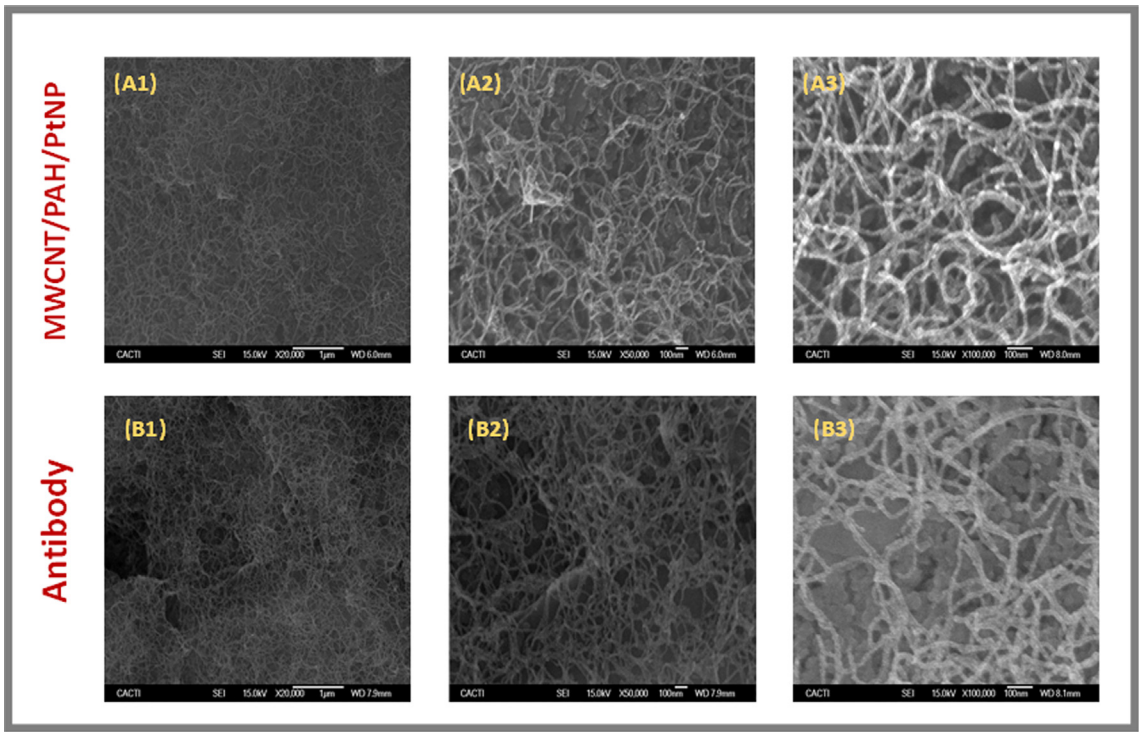

Fig. 4. SEM analysis of (A) MWCNTs-PAH/Pt with (A1) 20.000 times; (A2) 50.000 times and (A3) 100.000 times of magnification. (B) MWCNTs-PAH/Pt modified with the antibody with (B1) 20.000 times; (B2) 50.000 times and (B3) 100.000 times of magnification.

to be expected when the antibody is prepared in PBS buffer. Some sulfur is also detected, as it is part of some amino acids in the antibody. Pt and C are detected, but at low intensity due to the overlay from the antibody. Chlorine is still detected at low intensity due to the antibody overlay. The final stage of surface modification was to block the free amines on the sensor surface with BSA. As expected, an increase in oxygen and nitrogen content was observed due to the high oxygen content in BSA. Sodium, platinum and sulfur are detected, but with lower intensity due to the subsequent protein overlay.

After Tau protein binding, chlorine continued to be detected at low intensity due to the subsequent protein overlay. Oxygen increases due to the high oxygen content in the Tau protein, and the same occurs with nitrogen, which reaches a maximum. Chlorine and platinum continue to be detected at low intensity due to the subsequent protein overlay. Thus, the result is a maximum sulfur content and a minimum chlorine content. In conclusion, the XPS is sensitive to the changes and modifications made to the samples and the percentages agree quite well with the treatments performed.

3.3. Raman spectroscopy

Raman spectroscopy with a 532 nm laser makes it possible to verify structural information of carbon materials and their modifications. Raman spectra were recorded at different stages of the immunosensor assembly (**Figure S1**) (A) (pre)treatment, (B) incubation with the MWCNTs-PAH/Pt, (C) antibody binding, and (D) incubation with BSA.

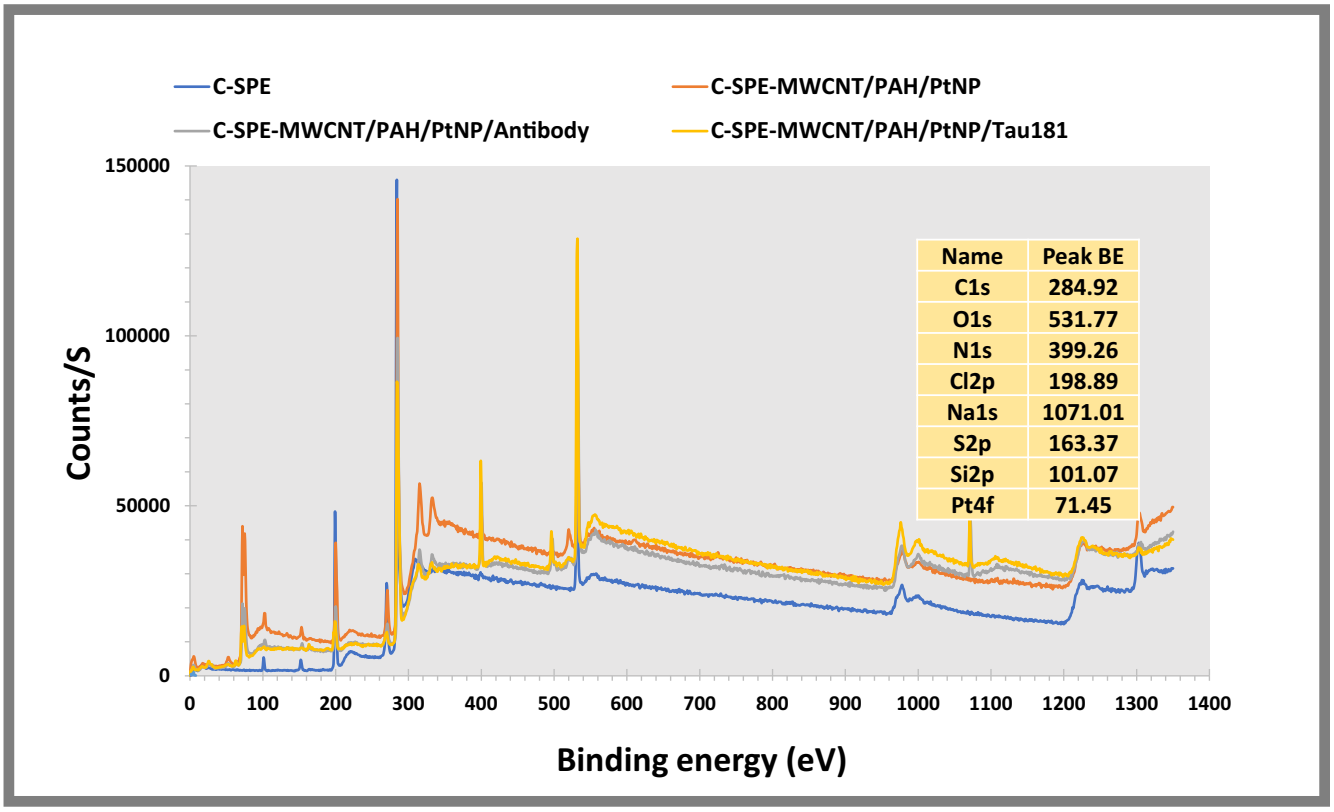

Fig. 5. XPS survey spectra of the C-SPE, MWCNTs-PAH/Pt, MWCNTs-PAH/Pt modified with the antibody and after p-Tau181 protein.

The positions, line shapes, and intensities of these peaks can be used to characterize the structures and properties of the immunosensor surface. Characteristic peaks for carbon-based materials were found in all spectra, such as the G' peak at 2700 cm^{-1}, the G peak at 1600 cm^{-1}, and the D peak at 1350 cm^{-1}. The D peak represents the presence of some disorder in the graphene structure related to the sp2 carbon bonds. While the G band is related to the sp3 carbon bonds. The intensity of the D band in relation to the G band is used as a measure of the quality of the nanotubes, i.e., it is possible to verify the presence of chemical changes based on the ratio I_D /I_G, quantifying the disorder of the material.

The results show that the intensity of the D peak increases with the modification of the electrode surface, indicating the presence of disorder in the carbon materials. After (pre) treatment of the electrode, an increase in disorder is observed (I_D /I_G 0.81 to 0.88). This could be due to the over-oxidation of the electrode and the resulting formation of carboxyl, carbonyl or aldehyde groups, which change the intrinsic properties of the graphite by altering the sp2 atomic structure and converting part of the graphite structure into new amorphous carbon. After casting the MWCNTs-PAH/Pt on the C-SPE surface, the I_D /I_G further increases. This could be due to the chemical modification of MWCNTs, which causes some defects in the structure. After antibody immobilization, we observed a slight decrease in the defects on the surface, which could be due to the presence of the antibodies on the surface. Overall, the difference in intensity between modifications serves as an indicator that the surface is altered.

3.4. Analytical performance of the immunoassay

3.4.1. Calibration curve in buffer

The electroanalytical performance of the immunosensor was evaluated using SWV in the presence of different concentrations of p-Tau181. As shown in Fig. 6A, an increase in the concentration of p-Tau181 leads to a decrease in current. Fig. 6B shows the calibration curve (current versus log[p-Tau181]) with a linear range starting at 8.6 to 1100 pg/mL. These tests were performed in buffer and yielded the following regression equation and correlation coefficient: I = -0.918(log[p-Tau181]) + 5.0871 and 0.9904. In this case, the detection limit was 0.24 pg/mL. The analytical performance of the electrode was evaluated in parallel with the nanocomposite modified C-SPE without nanoparticles (MWCNTs-PAH) and with the dendritic PtNP modified electrode (MWCNTs-PAH/dPt).

The electrode modified with the nanocomposite containing the dendritic nanoparticles showed a lower slope, I = -0.255(log[p-Tau181]) + 5.776. The slope of the calibration curve decreased by 74% compared to the biosensor modified with the spherical NP. Moreover, when the C-SPE is modified with MWCNTs/PAH without nanoparticles, a random behavior was observed. These results indicate that the morphology and the presence of nanoparticles are crucial for the success of a biosensor.

3.5. Application of immunosensor in the analysis of serum samples

To evaluate the performance of detection of p-Tau181 protein in serum, assays were performed using the same method as buffer calibration with different concentrations of p-Tau181 (8.6 to 1100 pg/mL in a 100 and 10-fold diluted FBS. This study, also performed in SWV, showed similar behavior to the calibration in buffer. The peak current decreases with the increase of p-Tau181 concentration. The study, performed at 100-fold dilution, yielded the following regression equation and correlation coefficient: I = -0.901(log[p-Tau181]) + 5.103 and 0.996, respectively (**Figure S2**). The other assay with 10-fold dilution gave the following regression equation and correlation coefficient I = -0.507(log[p-Tau181]) + 4.404 and 0.982, respectively (**Figure S2**). Both assays showed a decrease in terms of slope compared with the assay per-

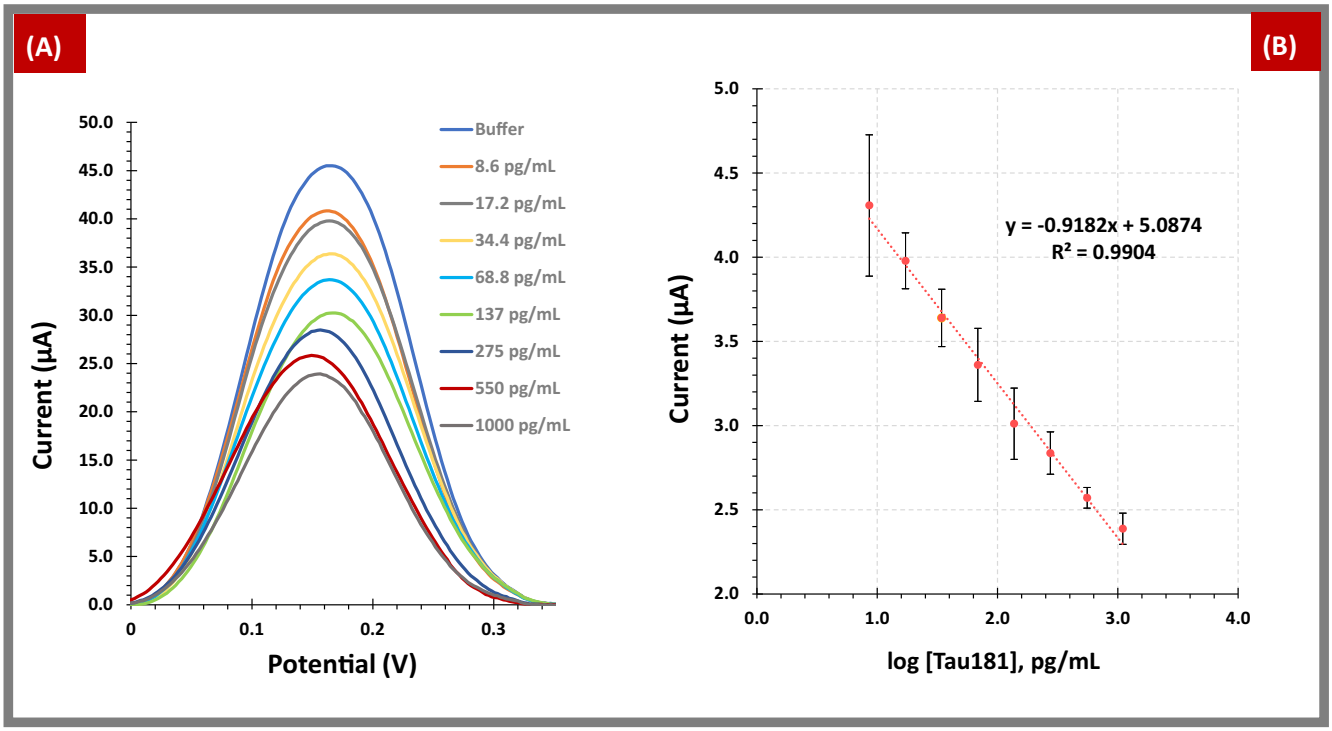

Fig. 6. Calibration curve in PBS buffer pH 7.4. (A) SWV measurements and (B) calibration curve logarithm of the concentration of p-Tau181 protein against current (µA). The electrochemical readings were performed in 5 mM $[Fe(CN)_6]^{3-/4-}$ prepared in KCl 0.1 M at scan rate 25 mVs^{-1}.

formed in buffer, although this decrease was greater for the assay using 10-fold diluted serum, but both assays maintained a linear response. Overall, this device showed a controlled response against p-Tau181 in a complex background such as FBS, indicating the ability to generate accurate data for serum sample analysis.

3.6. Selectivity study

The interference of other compounds was used to evaluate the selectivity of the immunosensor using SWV measurements. BSA, uric acid, hemoglobin, and IgG were selected as interfering substances corresponding to the normal composition of serum samples. The concentrations indicated were 4 mg/mL, 0.035 mg/mL, 7.4 mg/mL, and 100 µg/mL, respectively. Each solution was incubated in the sensor layer for 30 minutes, the same time specified for the standard solutions in the calibration procedure. These compounds were tested in a binary solution (interfering species and p-Tau181) in 100-fold diluted serum and compared with a solution containing only the p-Tau181 protein (30 pg/mL). The results obtained are presented in Fig. 7 and show a greater interference of uric acid (8%), followed by IgG(7%), hemoglobin (4%), and BSA (4%).

Overall, the obtained results demonstrate the good selectivity properties of the sensor layer and confirm the high affinity of the immunosensor for the p-Tau181 protein in the presence of potential interfering substances.

3.7. Spiked serum samples analysis

The standard addition method was used to determine Tau protein in spiked, diluted serum samples with p-Tau181 concentrations of 7.8 pg/mL, 15.6 pg/mL, and 1.0 ng/mL. This was performed in triplicate. Good agreement was obtained between the added and detected levels of p-Tau181, with recoveries within 87.0 and 95.0%, respectively (Table 1).

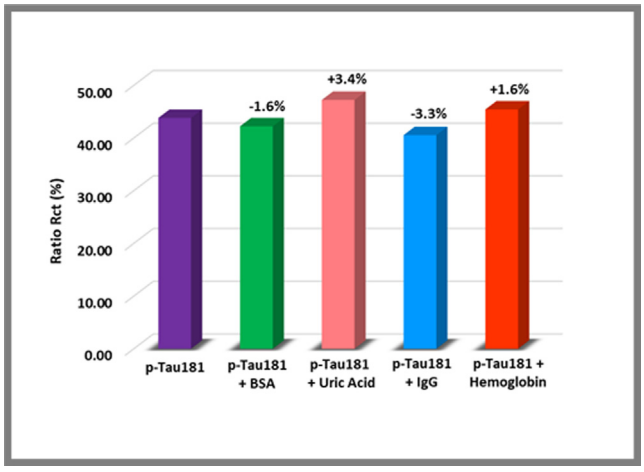

Fig. 7. Selectively study by mixed solution method. The interfering species were BSA, uric acid, IgG and hemoglobin.

Table 1
Results obtained from the recovery assay.

Added amount (pg/mL)	Found amount (pg/mL)	Recovered (%)
7.8	7.4	95.0
15.6	17.6	87.0
1000	909.8	91.0

4. Conclusions

We have successfully developed an ultrasensitive electrochemical immunosensor for a biomarker of Alzheimer's disease, p-Tau181 protein, for PoC analysis. The method combines the syn-

thesis of a composite nanomaterial with multi-walled CNTs modified with a polymer (PAH) and spherical Pt nanoparticles. In this work, the composite material with spherical nanoparticles showed better electrochemical performance than the dendritic counterparts or the CNTs without nanoparticles and was therefore used as a carrier for loading large amounts of antibodies and Pt nanoparticles for signal amplification. The proposed immunosensor provided excellent performance for the detection of p-Tau181 with LOD of 0.24 pg/mL in a concentration range of 8.6 pg/mL to 1100 pg/mL. Other devices reported in the literature have lower detection limits than those presented in this work, but we present a very simple and sensitive approach. Although the concentration of the protein p-Tau181 in the blood of healthy individuals is approximately 8 pg/mL, and higher values are expected in patients with AD. Thus, the sensitivity of the immunosensor presented in this work is sufficient to distinguish AD patients from healthy individuals.

In general, the developed device showed good analytical results for the detection of the protein p-Tau181. In addition to all the advantages, this immunosensor is portable and responds quickly, effectively, and easily to perform. Therefore, this device can contribute to PoC diagnoses to characterize and complement the AD diagnoses.

Declaration of Competing Interest

The authors declare that they have no known competing financial interests or personal relationships that could have appeared to influence the work reported in this paper.

Acknowledgements

Authors acknowledge funding to POCTEP through the project 2IQBioneuro with the reference (0624_2IQBIONEURO_6_E), entitled, Promotion of an R&I network in biological chemistry for the diagnosis and treatment of neurological diseases, EP-INTERREG V Spain Portugal (POCTEP).

Appendix A. Supplementary material

Supplementary data to this article can be found online at https://doi.org/10.1016/j.bioelechem.2022.108057.

References

[1] A. Europe, Dementia in Europe Yearbook: National policies covering the care and support of people with dementia and theircarers, Alzheimer Europe, 2013.
[2] European Commission. (2009). *Communication from the Commission to the European Parliament and the Council on a European initiative on Alzheimer's disease and other dementias.* European Commission.
[3] https://www.alzint.org/resource/numbers-of-people-with-dementia-worldwide/
[4] H. Brodaty, J. Clarke, M. Ganguli, A. Grek, A.F. Jorm, Z. Khachaturian, P. Scherr, Screening for cognitive impairment in general practice: Toward a consensus, Alzheimer Dis. Assoc. Disord. 12 (1) (1998) 1–13.
[5] E.M. Pfeiffer, R. Higdon, T.D. Koepsell, A.L. Fitzpatrick, D.L. Beekly, W.A. Kukull, Examining the agreement between CERAD and NIA/Reagan Institute neuropathological criteria for the diagnosis of Alzheimer's disease, Neurobiol. Aging 25 (2) (2004).
[6] B. Dubois, H. Feldman, P. ScheltenS, New criteria for the diagnosis of Alzheimer's disease, Neurobiol. Aging 29 (2008).
[7] N.C. Cullen, H. Zetterberg, P.S. Insel, B. Olsson, U. Andreasson, K. Blennow, O. Hansson, N. Mattsson-Carlgren, N. Alzheimer's Dis, Comparing progression biomarkers in clinical trials of early Alzheimer's disease, Annals of Clinical and Translational Neurology 7(9)(2020) 1661-1673.
[8] K. Blennow, H. Zetterberg, Biomarkers for Alzheimer's disease: current status and prospects for the future, J. Intern. Med. 284 (6) (2018) 643–663.
[9] A. Rabbito, M. Dulewicz, A. Kulczynska-Przybik, B. Mroczko, Biochemical Markers in Alzheimer's Disease, Int. J. Mol. Sci. 21 (6) (2020) 1–11.
[10] M. Dani, D.J. Brooks, P. Edison, Tau imaging in neurodegenerative diseases, Eur. J. Nucl. Med. Mol. Imaging 43 (6) (2016) 1139–1150.
[11] A. Anoop, P.K. Singh, R.S. Jacob, S.K. Maji, CSF Biomarkers for Alzheimer's Disease Diagnosis, Int. j. Alzheimer's disease 2010 (2010) 1–12.
[12] D.M. Holtzman, CSF biomarkers for Alzheimer's disease: current utility and potential future use, Neurobiol. Aging 32 (1) (2011) S4–S9.
[13] A.Z. Herskovits, A.J. Ivinson, C.R. Scherzer, B.T. Hyman, N. Lindeman, CSF and Blood Biomarkers for Alzheimer's Disease, Am. J. Clin. Pathol. 138 (3) (2012).
[14] N.R. Barthélemy, F. Fenaille, C. Hirtz, N. Sergeant, S. Schraen-Maschke, J. Vialaret, L. Buée, A. Gabelle, C. Junot, S. Lehmann, F. Becher, Tau Protein Quantification in Human Cerebrospinal Fluid by Targeted Mass Spectrometry at High Sequence Coverage Provides Insights into Its Primary Structure Heterogeneity, J. Proteome Res. 15 (2) (2016) 667–676.
[15] S. Shekhar, R. Kumar, N. Rai, V. Kumar, K. Singh, A.D. Upadhyay, M. Tripathi, S. Dwivedi, A.B. Dey, S. Dey, P. Garg, Estimation of Tau and Phosphorylated Tau (181) in Serum of Alzheimer's Disease and Mild Cognitive Impairment Patients, PLoS ONE 11 (7) (2016) e0159099, https://doi.org/10.1371/journal.pone.0159099.
[16] M.M. Mielke, C.E. Hagen, J. Xu, X. Chai, P. Vemuri, V.J. Lowe, D.C. Airey, D.S. Knopman, R.O. Roberts, M.M. Machulda, C.R. Jack, R.C. Petersen, J.L. Dage, Plasma phospho-tau181 increases with Alzheimer's disease clinical severity and is associated with tau- and amyloid-positron emission tomography, Alzheimers & Dementia 14 (8) (2018) 989–997.
[17] C.-C. Yang, M.-J. Chiu, T.-F. Chen, H.-L. Chang, B.-H. Liu, S.-Y. Yang, Assay of Plasma Phosphorylated Tau Protein (Threonine 181) and Total Tau Protein in Early-Stage Alzheimer's Disease, Journal of Alzheimers Disease 61 (4) (2018) 1323–1332.
[18] H. Tatebe, T. Kasai, T. Ohmichi, Y. Kishi, T. Kakeya, M. Waragai, M. Kondo, D. Allsop, T. Tokuda, Quantification of plasma phosphorylated tau to use as a biomarker for brain Alzheimer pathology: pilot case-control studies including patients with Alzheimer's disease and down syndrome, Mol. Neurodegener. 12 (63) (2017) 1–11.
[19] S.X.Y. Wang, D. Acha, A.J. Shah, F. Hills, I. Roitt, A. Demosthenous, R.H. Bayford, Detection of the tau protein in human serum by a sensitive four-electrode electrochemical biosensor, Biosens. Bioelectron. 15 (92) (2017) 482–488.
[20] A. Lleo, H. Zetterberg, J. Pegueroles, T.K. Karikari, M. Carmona-Iragui, N.J. Ashton, V. Montal, I. Barroeta, J. Lantero-Rodriguez, L. Videla, M. Altuna, B. Benejam, S. Fernandez, S. Valldeneu, D. Garzon, A. Bejanin, M.F. Iulita, V. Camacho, S. Medrano-Martorell, O. Belbin, J. Clarimon, S. Lehmann, D. Alcolea, R. Blesa, K. Blennow, J. Fortea, Phosphorylated tau181 in plasma as a potential biomarker for Alzheimer's disease in adults with Down syndrome, Nat. Commun. 12 (1) (2021) 1–8.
[21] A.P.F. Turner, Biosensors: sense and sensibility, Chem. Soc. Rev. 42 (8) (2013) 3184–3196.
[22] X.X. Fan, D.M. Deng, Z.C. Chen, J. Qi, Y.Y. Li, B.S. Han, K. Huan, L.Q. Luo, A sensitive amperometric immunosensor for the detection of carcinoembryonic antigen using ZnMn2O4@reduced graphene oxide composites as signal amplifier, Sens.Actuators B-Chem. 339 (2021) 129852.
[23] Y. Chen, Y.u. Li, D. Deng, H. He, X. Yan, Z. Wang, C. Fan, L. Luo, Effective immobilization of Au nanoparticles on TiO2 loaded graphene for a novel sandwich-type immunosensor, Biosens. Bioelectron. 102 (2018) 301–306.
[24] M.A. Garcia-Chame, O. Gutierrez-Sanz, E. Ercan-Herbst, N. Haustein, M.S. Filipiak, D.E. Ehrnhofer, A. Tarasov, A transistor-based label-free immunosensor for rapid detection of tau protein, Biosens. Bioelectron. 1 (159) (2020) 1–6.
[25] V. Maurer, C. Frank, J.C. Porsiel, S. Zellmer, G. Garnweitner, R. Stosch, Step-by-step monitoring of a magnetic and SERS-active immunosensor assembly for purification and detection of tau protein, J. Biophotonics 13 (3) (2020) 1–10.
[26] C.A. Razzino, V. Serafin, M. Gamella, M. Pedrero, A. Montero-Calle, R. Barderas, M. Calero, A.O. Lobo, P. Yanez-Sedeno, S. Campuzano, J.M. Pingarron, An electrochemical immunosensor using gold nanoparticles-PAMAM-nanostructured screen-printed carbon electrodes for tau protein determination in plasma and brain tissues from Alzheimer patients, Biosens. Bioelectron. 163 (2020) 112238.
[27] B. Shui, D. Tao, J. Cheng, Y. Mei, N. Jaffrezic-Renault, Z. Guo, A novel electrochemical aptamer-antibody sandwich assay for the detection of tau-381 in human serum, Analyst 143 (15) (2018) 3549–3554.
[28] A. Ben Hassine, N. Raouafi, F.T.C. Moreira, Novel Electrochemical Molecularly Imprinted Polymer-Based Biosensor for Tau Protein Detection, Chemosensors 9 (9) (2021) 1–14.
[29] L.M.T. Phan, T.X. Hoang, T.A.T. Vo, H.L. Pham, H.T.N. Le, S.R. Chinnadayyala, J.Y. Kim, S.M. Lee, W.W. Cho, Y.H. Kim, S.H. Choi, S. Cho, Nanomaterial-based Optical and Electrochemical Biosensors for Amyloid beta and Tau: Potential for early diagnosis of Alzheimer's Disease, Exp. Rev. Mol. Diagnostics 21 (2) (2021) 175–193.
[30] S. Lisi, S. Scarano, S. Fedeli, E. Pascale, S. Cicchi, C. Ravelet, E. Peyrin, M. Minunni, Toward sensitive immuno-based detection of tau protein by surface plasmon resonance coupled to carbon nanostructures as signal amplifiers, Biosens. Bioelectron. 93 (2017) 289–292.
[31] N. Carlin, S. Martic-Milne, Anti-Tau Antibodies Based Electrochemical Sensor for Detection of Tau Protein Biomarkers, J. Electrochem. Soc. 165 (12) (2018) G3018–G3025.
[32] M.N.S. Karaboga, M.K. Sezginturk, Analysis of Tau-441 protein in clinical samples using rGO/AuNP nanocomposite-supported disposable impedimetric

neuro-biosensing platform: Towards Alzheimer's disease detection, Talanta 219 (2020) 121257.
[33] P. Joshi, R. Mishra, R.J. Narayan, Biosensing applications of carbon-based materials, Current Opinion Biomed. Eng. 18 (2021) 100274, https://doi.org/10.1016/j.cobme.2021.100274.
[34] A.K. Trilling, J. Beekwilder, H. Zuilhof, Antibody orientation on biosensor surfaces: a minireview, Analyst 138 (6) (2013) 1619–1627.
[35] M. Wilchek, T. Miron, Oriented versus random protein immobilization, J. Biochem. Bioph. Methods 55 (1) (2003) 67–70.